

3D Human Pose Analysis via Diffusion Synthesis

Haorui Ji¹, Hongdong Li¹

¹The Australian National University
{haorui.ji, hongdong.li}@anu.edu.au

Abstract

Diffusion models have demonstrated remarkable success in generative modeling. In this paper, we propose PADS (Pose Analysis by Diffusion Synthesis), a novel framework designed to address various challenges in 3D human pose analysis through a unified pipeline. Central to PADS are two distinctive strategies: i) learning a task-agnostic pose prior using a diffusion synthesis process to effectively capture the kinematic constraints in human pose data, and ii) unifying multiple pose analysis tasks like estimation, completion, denoising, etc. as instances of inverse problems. The learned pose prior will be treated as a regularization imposing on task-specific constraints, guiding the optimization process through a series of conditional denoising steps. PADS represents the first diffusion-based framework for tackling general 3D human pose analysis within the inverse problem framework. Its performance has been validated on different benchmarks, signaling the adaptability and robustness of this pipeline.

1 Introduction

3D human pose analysis (3D HPA) generally refers to the task of analysing or reconstructing 3D human poses under different conditions. Typical tasks include for human pose estimation, pose completion, motion generation, etc. Its practical significance extends to various human-centered applications, such as human-computer interaction, virtual reality, sports analysis, and healthcare [Jiang *et al.*, 2022; Weng *et al.*, 2019; Stenum *et al.*, 2021].

Most existing pose analysis methods focus on training deep neural networks over paired datasets comprising 3D human poses and the corresponding conditions. While these models demonstrate superior performance in terms of both reconstruction accuracy and inference speed, their advantages are constrained by two notable drawbacks: 1) Dependency on access to a substantial volume of paired data, and 2) Limitation to the application scope defined by the domain of the training data.

In order to bypass these downsides, there has been an increasing interest in developing a general pose analysis ca-

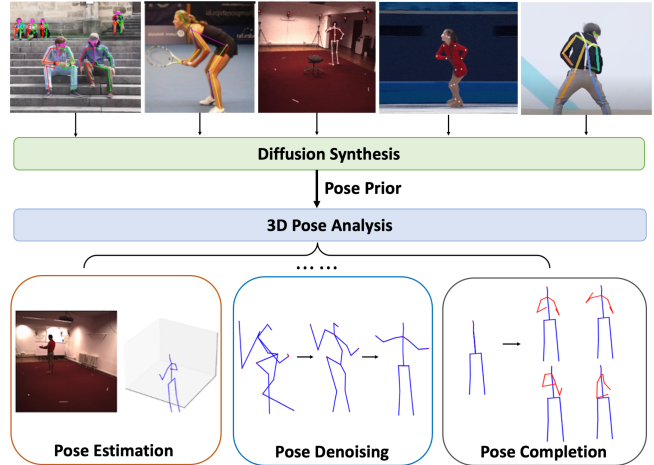


Figure 1: Learned pose prior can be used to discriminate infeasible solutions and address noise sensitivity. Its applications span across various pose analysis tasks such as 3D pose estimation from 2D, denoising 3D poses, recovering missing parts on human skeleton, and plausible poses generation.

pability without the necessity for task-specific high-quality paired dataset preparation. To achieve this goal, obtaining a well-defined prior distribution, who exploits the inherent spatial structure in human skeletons, is deemed essential. Fig.1 exhibits some use cases where pose priors can be effectively applied.

Researchers have explored different ways to incorporate prior knowledge of human bodies into pose analysis. [Hatze, 1997] explicitly defines joint-angle limits, yet configuring complete kinematic constraints for each joint has been proven challenging. Data-driven priors have also been proposed [Loper *et al.*, 2023; Davydov *et al.*, 2022; Ci *et al.*, 2023] by characterizing the distribution of authentic 3D human poses. Effective as they are, these methods often necessitate additional efforts to integrate task-specific constraints when applied to downstream tasks, leading to efficiency degradation.

In this paper, we introduce PADS (Pose Analysis by Diffusion Synthesis), offering a novel perspective on modeling human pose prior using diffusion synthesis and applying the learned prior to general pose analysis purposes in

an unified diffusion-based inverse problem manner, whose ill-posed nature makes it a perfect mathematical tool for characterizing 3D pose analysis problems. Recently, diffusion models’ proficiency of modeling complex data distribution makes it a good candidate for solving inverse problems, particularly in a zero-shot pipeline [Li *et al.*, 2023]. However, many diffusion-based approaches focus primarily in the image processing domain, such as inpainting, super-resolution, deblurring [Choi *et al.*, 2021; Kwar *et al.*, 2022; Song *et al.*, 2022], etc., limiting their applicability to more general usage scenarios. To the best of our knowledge, similar methods have not been yet deployed in 3D human pose area and our paper is the first to fill in this research gap.

To summarize, our contributions are as follows:

- This paper introduces PADS, a novel framework that tackles various pose analysis problems in a unified diffusion-based pipeline.
- PADS models 3D human pose prior through diffusion synthesis process and formulates various pose analysis tasks as instances of general inverse problems. Taking advantage of diffusion-based inverse problem solver and injecting pretrained pose prior, PADS enables to optimize for the corresponding 3D human skeleton given different conditions.
- PADS achieves state-of-the-art performances across multiple benchmarks, underscoring its effectiveness of the diffusion-based prior representation as well as solving 3D pose analysis tasks within the inverse problem framework.

2 Related Work

2.1 3D Human Pose Analysis

3D human pose analysis encompasses multiple tasks, producing corresponding 3D poses under different conditions such as observed 2D pose, occluded 3D pose, pure noise, etc. In this context, we define “pose” as a set of predetermined key-points that forms the basic skeleton of human body, and the terms “pose” and “skeleton” will be used interchangeably without loss of generality.

Conventional methods often involve direct end-to-end learning of condition-to-pose mapping through diverse network designs. [Martinez *et al.*, 2017] proposes a simple yet effective MLP-based neural network trained on single-frame 2D-3D poses pair. Building upon this, [Pavlo *et al.*, 2019] extends the concept to accommodate sequence input, exploiting the usage of temporal information. Transformers have also been introduced for addressing sequential 3D pose analysis challenges [Li *et al.*, 2022; Zhang *et al.*, 2022] and achieve state-of-the-art performance.

To resolve the depth ambiguity issue when predicting human skeletons, generative representations have been utilized to facilitate the modeling of 3D human pose priors. SMPL-oriented methods [Bogo *et al.*, 2016; Kanazawa *et al.*, 2018] focus on designing optimizers to output human poses that fit the predefined shape model. GAN-based methods [Chen *et al.*, 2019; Davydov *et al.*, 2022; Kocabas *et al.*, 2020] learn adversarial priors by discriminating generated poses from real

ones. Alternative priors as well as data augmentations such as random rotation perturbation [Novotny *et al.*, 2019], low-rank property [Ji *et al.*, 2023], etc., have also been considered to enforce the plausibility of predicted human poses. However, when applying these task-independent priors to downstream analysis tasks, separate task-specific networks are usually required and additional efforts on balancing prior terms and target objectives will become inevitable.

PADS not only leverages the power of emerging diffusion-based generative modeling but also enhances the efficiency of prior-based pose analysis pipeline by formulating pose-related tasks as general inverse problems. The learned prior is considered as a plugin in the optimization process and doesn’t need the involvement of task-specific networks when applying to downstream tasks. In comparison to GFPose [Ci *et al.*, 2023], another similar work utilizing a diffusion scheme to model pose prior, PADS differs in its condition strategy. GFPose injects task-specific conditions in the network design and focuses on learning a task-aware pose prior via supervised manner. In contrast, PADS only incorporates conditions during the inference stage, eliminating the need for paired data preparation and enabling easy adaptation to new scenarios without retraining.

2.2 Diffusion for Generative Modeling

Diffusion models are a class of generative models designed implement generative modeling through a sequence of noising and denoising processes. [Song *et al.*, 2020c] first defines a stochastic differential equation (SDE) that can transform complex data distributions to a known prior by progressively injecting noise. Notably, original distributions can be restored by solving the corresponding reverse-time SDE from $t = T$ back to $t = 0$.

$$d\mathbf{x} = \left[-\frac{\beta(t)}{2}\mathbf{x} - \beta(t)\nabla_{\mathbf{x}_t} \log p_t(\mathbf{x}_t) \right] dt + \sqrt{\beta(t)}d\bar{\mathbf{w}} \quad (1)$$

where $\nabla_{\mathbf{x}_t} \log p_t(\mathbf{x}_t)$, also known as score functions, represents the gradient of the log probability densities with respect to data, β_t is the schedule of the noising process, and $\bar{\mathbf{w}}$ is a standard Wiener process.

The versatility of diffusion models in modeling complex data distributions has led to remarkable achievements across various research domains, including visual content generation [Rombach *et al.*, 2022], as well as detection and segmentation [Chen *et al.*, 2023]. Recent applications have expanded to 3D vision tasks, such as 3D reconstruction [Poole *et al.*, 2022; Shan *et al.*, 2023] and motion generation [Tevet *et al.*, 2022; Yuan *et al.*, 2023].

Diffusion models not only excel in capturing unconditional data distribution but are also adept at modeling conditional ones. Based on the training strategy, these works can be divided into two categories. The first category is dedicated to optimizing the diffusion model from scratch via supervised learning. This setup facilitates controlled generation processes based on multiple conditions such as text [Zhang *et al.*, 2023], pose [Ma *et al.*, 2023], or other images [Ho and Salimans, 2022], etc. In the second paradigm, conditioning is introduced through Bayes’ theorem where var-

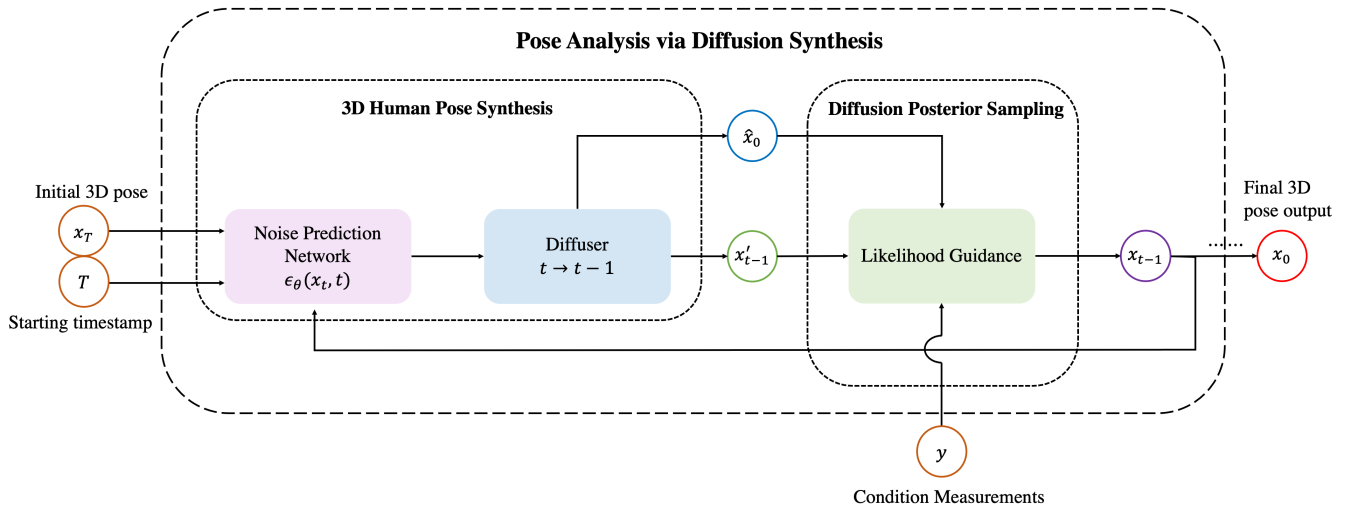


Figure 2: Overview of the PADS framework. The whole framework consists of two stages. In the training stage, we train a diffusion-based 3D human pose synthesis network to model the underlying kinematic constraints from real pose data. In the inference stage, we utilize this learned prior along with an inverse problem solver to inject likelihood guidance into the sampling process.

ious techniques [Choi *et al.*, 2021; Kavar *et al.*, 2022; Chung *et al.*, 2022a; Song *et al.*, 2022] are developed to inject conditions in the sampling process, generating samples from the target conditional distribution. Despite facing challenges in performance compared to supervised approaches, these ”plug-and-play” methods are more desirable for practical use due to their superior generalization abilities.

3 Method

3.1 Problem Formulation

Different downstream tasks included in 3D pose analysis domain can be unified by modeling conditional data distributions $p(\mathbf{x}|\mathbf{c})$ where $\mathbf{x} \in \mathbb{R}^{J \times 3}$ represents the 3D pose of a human skeleton and \mathbf{c} are different task conditions. In pose estimation, $\mathbf{c} \in \mathbb{R}^{J \times 2}$ denotes 2D poses. It uses either a single frame or a sequence of 2D poses as input to locate the 3D positions of human body joints. In pose denoising and pose completion, $\mathbf{c} \in \mathbb{R}^{J \times 3}$ is the unsatisfied 3D poses, either jittered by noise or partially-occluded to present incomplete human skeletons. For pose generation, $\mathbf{c} \in \emptyset$ as it aims for unconstrained synthesis.

3.2 Pose Analysis as Inverse Problems

The core of PADS is to formulate instances of 3D pose analysis as non-linear inverse problems and subsequently solving them within a unified generative pipeline, i.e. generating samples from target conditional distributions. For general inverse problems, we consider a signal $\mathbf{x} \in \mathbb{R}^n$ and its corresponding measurement $\mathbf{y} \in \mathbb{R}^m$, whose relationship can be expressed as:

$$\mathbf{y} = f(\mathbf{x}) + \mathbf{n}, \quad \mathbf{y} \in \mathbb{R}^m \quad \mathbf{x}, \mathbf{n} \in \mathbb{R}^n, \quad (2)$$

where $f(\cdot) : \mathbb{R}^n \rightarrow \mathbb{R}^m$ is the forward measurement operator transforming from signal space to measurement space, and $\mathbf{n} \in \mathbb{R}^n$ represents the measurement noise. In the 3D pose

analysis setup, we’ll reuse the notations in Sec.3.1, where skeletons \mathbf{x} represent original signals, conditions \mathbf{c} represent measurements, and f serve as measurement operators varying according to different tasks. For instance, in pose estimation, $f(\cdot) : \mathbb{R}^3 \rightarrow \mathbb{R}^2$ is the perspective camera projection process given camera intrinsics. In pose denoising, $f(\cdot) : \mathbb{R}^3 \rightarrow \mathbb{R}^3$ corresponds to the imposition of predefined noise. In pose completion, $f(\cdot) : \mathbb{R}^3 \rightarrow \mathbb{R}^3$ is the masking process.

3.3 General Framework

In the context of diffusion models, solving a time-reverse SDE with the learned score function will reduce to sampling from the corresponding distribution. Therefore, it is straightforward to modify the original SDE in Eqn.1 accordingly to adapt it for conditional sampling and arrive at the desired reverse diffusion sampler.

$$d\mathbf{x} = \left[-\frac{\beta(t)}{2} \mathbf{x} - \beta(t) \nabla_{\mathbf{x}_t} \log p_t(\mathbf{x}_t|\mathbf{y}) \right] dt + \sqrt{\beta(t)} d\bar{\mathbf{w}}, \quad (3)$$

The posterior scores can be further decomposed into the combination of a prior term and a likelihood term based on Bayes’ theorem

$$\nabla_{\mathbf{x}_t} \log p_t(\mathbf{x}_t|\mathbf{y}) = \nabla_{\mathbf{x}_t} \log p_t(\mathbf{x}_t) + \nabla_{\mathbf{x}_t} \log p_t(\mathbf{y}|\mathbf{x}_t). \quad (4)$$

where the first term can be approximated using unconditional diffusion modeling and the second term represents guidance from the conditioning likelihood to ensure generated samples satisfy forward measurement constraints. According to this decomposition, PADS designs a two-stage pipeline: 1) In the training stage, we train an unconditional diffusion network to model the underlying prior score of data; 2) In the inference stage, we utilize this learned prior along with an off-the-shelf inverse problem solver to inject likelihood guidance into the sampling process to impose data consistency. Fig.2 describes a general framework that follows the strategy introduced above, and the following sections will dive into each component in more detail.

3.4 Pose Diffusion Synthesis

The initial step involves obtaining a robust task-independent pose prior by training a diffusion-based 3D human pose synthesis network. Our model considers pelvis joint as root and synthesize the relative-to-pelvis 3D poses to focuses primarily on the shape of human skeleton rather than its global trajectory. By reconstructing input poses in a denoising autoencoding manner, we compel the diffusion model to learn effective kinematic constraints from genuine 3D poses.

In this work, we employ the Denoising Diffusion Probabilistic Models (DDPM) sampling scheme [Ho *et al.*, 2020] for the pose synthesis model, who consists of a forward diffusion process and a reverse sampling process. The forward process continuously corrupts the ground truth 3D pose \mathbf{x}_0 with independent noise ϵ_t , producing a sequence of intermediate noisy samples $\mathbf{x}_1, \mathbf{x}_2, \dots, \mathbf{x}_T$ that constructs a Markov chain with a Gaussian transition kernel $q(\mathbf{x}_t|\mathbf{x}_{t-1})$. When T is sufficiently large, the latent \mathbf{x}_T is nearly identical to an isotropic Gaussian distribution. Conversely, the reverse process gradually removes noise in the reverse time direction through a Markov chain with learnable Gaussian transition kernel $p_\theta(\mathbf{x}_{t-1}|\mathbf{x}_t)$.

Following [Ho *et al.*, 2020], our synthesis network predicts the added noise in the forward diffusion process $\epsilon_\theta(\mathbf{x}_t, t)$ that indicates how much denoising should be applied to \mathbf{x}_t . This is implemented using a Transformer encoder-based architecture, whose innovative attention-based design is suitable for non-structural feature aggregation. By computing the attention between joints, our network is able to proficiently model dependencies in human skeletons regardless of spatial structures. The network overview is depicted in Fig.3. To reconstruct input pose that is consistent with the original data distribution, key is to make sure the learned reverse Markov chain matches the actual time reversal of the forward Markov chain. This alignment can be achieved by minimizing the KL divergence between the distributions $p_\theta(\mathbf{x}_{t-1}|\mathbf{x}_t)$ and $q(\mathbf{x}_{t-1}|\mathbf{x}_t)$ at every timestamp. Therefore the final loss function is formulated as

$$\begin{aligned} L &= \mathbb{E}_{t, \mathbf{x}_0, \epsilon_t} [D_{KL}(q(\mathbf{x}_{t-1}|\mathbf{x}_t) || p_\theta(\mathbf{x}_{t-1}|\mathbf{x}_t))] \\ &= \mathbb{E}_{t, \mathbf{x}_0, \epsilon_t} [\|\epsilon_t - \epsilon_\theta(\mathbf{x}_t, t)\|_2^2]. \end{aligned} \quad (5)$$

3.5 Diffusion Posterior Sampling

Following the decomposition in Eqn.4, the next step is to incorporate likelihood guidance in the sampling process to perform conditional sampling. Several methods have been proposed to approximate the intractable, time-dependent likelihood score. Our PADS framework is constructed upon the effective image restoration solver, Diffusion Posterior Sampling (DPS) [Chung *et al.*, 2022a], and generalize its concept for 3D pose analysis tasks. Specifically, DPS introduces an approximation quantified with the Jensen gap:

$$\nabla_{\mathbf{x}_t} \log p(\mathbf{y}|\mathbf{x}_t) \simeq \nabla_{\mathbf{x}_t} \log p(\mathbf{y}|\hat{\mathbf{x}}_0) = -\frac{1}{\sigma^2} \nabla_{\mathbf{x}_t} \|\mathbf{y} - f(\hat{\mathbf{x}}_0)\|_2^2, \quad (6)$$

where $\hat{\mathbf{x}}_0 = \mathbb{E}[\mathbf{x}_0|\mathbf{x}_t]$ equals the closed-form solution of posterior mean, σ is the variance of measurement noise, and $f(\cdot)$

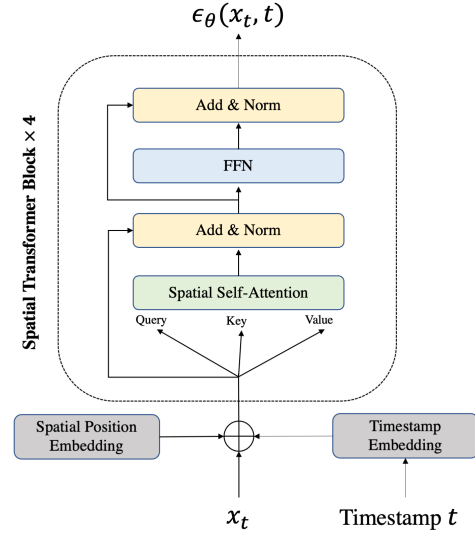


Figure 3: Overview of noise prediction network. Input is the perturbed pose vector and its corresponding timestamp in the diffusion chain. After being linearly embedded and adding spatial position embeddings, the resulting vector is sent to a stacked spatial encoder architecture and outputs the estimated noise that it has been applied.

is the corresponding forward measurement operator. Combining the above results with the learned pose prior obtained from Sec.3.4, we can conclude that

$$\nabla_{\mathbf{x}_t} \log p(\mathbf{x}_t|\mathbf{y}) \simeq -\frac{1}{\sqrt{1-\bar{\alpha}_t}} \epsilon_\theta(\mathbf{x}_t, t) - \rho \nabla_{\mathbf{x}_t} \|\mathbf{y} - f(\hat{\mathbf{x}}_0)\|_2^2, \quad (7)$$

where ρ is set as a hyperparameter that controls the scale of likelihood guidance.

PADS framework applies the DPS method to 3D pose analysis in the inference stage, resulting in effective zero-shot strategy capable of handle various downstream tasks without retraining additional models. We illustrate an example pipeline of utilizing PADS for 3D human pose estimation in Alg.1, and applications to other analysis tasks can be implemented in similar ways by only changing the measurement operator. The uniqueness of pose estimation lies in the non-linearity of perspective projection process. To remain consistent with the learned pose prior, we output relative-to-pelvis 3D poses in every sampling step and the global trajectory information will be input externally. Furthermore, motivated by [Zheng *et al.*, 2022], we propose a pose initialization strategy that instead of starting from pure Gaussian noise, we initiate the sampling process from the inverse projection of the 2D measurement pose given its root's global trajectory in order to truncate the diffusion chain and enhance sampling speed as well as accuracy. With a camera intrinsic K , 2D pose measurements, P_{2d} , and the root joint's global trajectory T , the initial pose P_{init} can be calculated using inverse perspective projection.

$$\begin{aligned} \tilde{P}_{init} &= \frac{K^{-1}P_{2d}}{\|K^{-1}P_{2d}\|_2} \|T\|_2, \\ P_{init} &= \tilde{P}_{init} - \tilde{P}_{init}^{pelvis}. \end{aligned} \quad (8)$$

Algorithm 1 PADS for 3D Human Pose Estimation

Require: 2D pose measurement P_{2d} ,
Camera intrinsic K ,
Pelvis root trajectory T ,
Number of diffusion sampling iterations N ,
Pose prior $\epsilon_\theta(\mathbf{x}_t, t)$
Guidance scale $\{\rho_t\}_{t=1}^N$, Noise variance $\{\sigma_t\}_{t=1}^N$
// Pose initialization
 $\tilde{P}_{init} \leftarrow \frac{K^{-1}P_{2d}}{\|K^{-1}P_{2d}\|_2} \|T\|_2$
 $P_{init} \leftarrow \tilde{P}_{init} - \tilde{P}_{init}^{pelvis}$
// Iterative reverse sampling
 $\mathbf{x}_N \leftarrow P_{init}$
 $\mathbf{y} \leftarrow P_{2d}$
for $t \leftarrow N$ **to** 1 **do**
 $\hat{\mathbf{x}}_0 \leftarrow \frac{1}{\sqrt{\alpha_t}}(\mathbf{x}_t - \sqrt{1 - \alpha_t}\epsilon_\theta(\mathbf{x}_t, t))$
 $\mathbf{z} \sim N(0, \mathbf{I})$
 $\mathbf{x}'_{t-1} \leftarrow \frac{\sqrt{\alpha_t}(1 - \bar{\alpha}_{t-1})}{1 - \bar{\alpha}_t} \mathbf{x}_t + \frac{\sqrt{\bar{\alpha}_{t-1}\beta_t}}{1 - \bar{\alpha}_t} \hat{\mathbf{x}}_0 + \sigma_t \mathbf{z}$
 $\mathbf{x}_{t-1} \leftarrow \mathbf{x}'_{t-1} - \rho_t \nabla_{\mathbf{x}_t} \|\mathbf{y} - proj(\hat{\mathbf{x}}_0)\|_2^2$
end for
return \mathbf{x}_0

4 Experiments

In this section, we present the experimental results of PADS framework. We will begin by introducing the datasets and evaluation metrics used in our study, followed by an overview of the implementation details. Subsequently, we will demonstrate the effectiveness of PADS under different tasks with qualitative and quantitative results. Finally, we will conduct detailed ablation studies to investigate the impact of various components of PADS under the problem setting of pose estimation.

4.1 Datasets and Evaluation Protocols

H36M [Ionescu *et al.*, 2013] is the most widely used indoor dataset for 3D human pose analysis. The dataset employs a multi-camera setup, capturing various types of daily activities from different angles in indoor environments and annotates them with 3D ground truth using motion capture systems. Following the convention from previous works, subjects S1, S5, S6, S7, and S8 are used as the training set, while S9 and S11 are used for testing.

MPI-INF-3DHP [Mehta *et al.*, 2017] is a recently popular dataset that features more complex scenarios, including indoor, green screen, and outdoor scenes. It records eight subjects performing multiple activities from 14 different views. We use the valid frames provided by the official dataset for testing.

Evaluation metrics. We report the mean per joint position error (MPJPE) in millimeters as the major metric, computed by measuring the Euclidean distance between the estimated pose and the ground truth pose. Additionally, Procrustean alignment MPJPE (PA-MPJPE), the MPJPE after rigid alignment post-processing, is also reported. For 3DHP datasets, additional metrics like percentage of correct keypoints (PCK) thresholded at 150mm and the area under the curve (AUC) are also included.

4.2 Implementation Details

In the training stage, the 3D pose synthesis model is trained for 100 epochs with batch size of 1024, learning rate 10^{-4} , and the AdamW optimizer. An exponential moving average strategy with ratio of 0.9999 is also adopted. For the diffusion process, we follow conventional DDPM training strategy, where the maximum iteration is set as $T = 1000$, the timestamp t is uniformly sampled from $[1, T]$, and the variances of added noises are configured to linearly increase from $\beta_1 = 10^{-4}$ to $\beta_T = 0.02$. All 3D human poses are normalized to pelvis-related coordinates. Our experiments are performed on one NVIDIA 4070Ti GPU, and the training takes about 12 hours to complete.

During inference, as suggested in Sec. 3.5, we truncate the complete diffusion chain to $T = 450$ and iteratively sample from back to $t = 0$ using the DDIM sampler in order to facilitate the sampling process. In every iteration, we fix the scale of the likelihood guidance to $\rho = 0.003$.

4.3 Pose Estimation

In this section, we verify how PADS can handle pose estimation, the core problem in pose synthesis with superior performance. PADS possesses several key properties: 1) it is an unsupervised method since the training process does not require any 2D-3D paired pose data. 2) it is an optimization-based method as it essentially treats the learned pose prior as a constraint and optimizes for the 3D pose through a sequence of sampling processes. 3) it operates under a single hypothesis setting, i.e., only one hypothesis is drawn during each sampling step. For a fair comparison, the experimental results are compared within methods that are characterized similarly.

As shown in Table 1, PADS achieves 41.5mm in MPJPE, 33.1mm in PA-MPJPE, outperforming any existing state-of-the-art (SOTA) methods in both categories by a significant margin, even comparable with some supervised or multi-hypothesis methods. Furthermore, PADS behaves well using either the ground truth or the noisy detected 2D keypoints as inputs, indicating its capability of generalization when facing unsatisfied task conditions.

We also report the results on 3DHP dataset. Following previous works, we use ground truth 2D poses as input. As shown in Table 2, PADS achieves 63.7mm in PA-MPJPE, 86.6 in PCK and 57.6 in AUC. Although existing some gap with SOTA in terms of PA-MPJPE, PADS can still achieve comparably good performance in overall metrics compared with both learning-based and optimization-based methods, which still demonstrates its effectiveness.

4.4 Pose Denoising

In real world applications, 3D human poses acquired from wearable devices or vision-based algorithms are likely to suffer from different types of defects. For example, motion capture data may be perturbed by noise, characters from metaverse applications may be occluded and thus have partial observations. In the following sections, we'll verify how PADS can be applied in such scenarios for remedy better 3D pose outputs with examples of pose denoising and pose completion. These two analysis tasks can both be modeled as linear

Mode	Method	GT		DT	
		MPJPE ↓	PMPJPE ↓	MPJPE ↓	PMPJPE ↓
Lrn.	[Yu <i>et al.</i> , 2021]	85.3	42.0	92.4	54.3
	[Wang and Lucey, 2021]	88.3	-	132.5	-
	[Zeng <i>et al.</i> , 2022]	72.6	-	-	-
	[Wandt <i>et al.</i> , 2022]	<u>64.0</u>	<u>36.7</u>	-	-
Opt.	[Bogo <i>et al.</i> , 2016]	82.3	-	-	-
	[Song <i>et al.</i> , 2020b]	-	56.4	-	-
	[Jiang <i>et al.</i> , 2023] ($H = 1$)	-	-	65.7	49.0
	[Jiang <i>et al.</i> , 2023] ($H = 10$)	-	-	<u>57.1</u>	<u>45.1</u>
	Ours	41.5	33.1	54.8	44.9

Table 1: 3D human pose estimation quantitative results on H36M dataset. All results are reported in millimeters (mm). *Lrn.* stands for learning-based methods and *Opt.* means optimization-based methods. *GT* and *DT* respectively denote results using ground truth 2D inputs and detected 2D pose by off-the-shelf 2D detector. H is the number of hypothesis. The best and second-best results are highlighted in bold and underline formats.

Method	PA-MPJPE ↓	PCK ↑	AUC ↑
[Chen <i>et al.</i> , 2019]	-	71.7	36.3
[Yu <i>et al.</i> , 2021]	-	<u>86.2</u>	<u>51.7</u>
[Wandt <i>et al.</i> , 2022]	54.0	86.0	50.1
[Jiang <i>et al.</i> , 2023]	86.5	82.6	53.8
Ours	<u>63.7</u>	86.6	57.6

Table 2: 3D HPE quantitative results on 3DHP dataset. Ground truth 2D keypoints inputs are used. The best and second-best results are highlighted in bold and underline formats.

Noise Type	Intensity	Before ↓	After ↓
Gaussian	25%	75.3	51.6
	50%	150.5	63.8
	100%	301.2	88.7
Uniform	25%	45.2	43.1
	50%	90.4	52.9
	100%	180.9	69.6

Table 3: Pose denoising results on H36M dataset. The noise intensity is calculated based on the average bone length of human body. We report the MPJPE (mm) metric before and after denoising action

inverse problems, thus PADS is able to resolve them in similar ways.

The forward operator for denoising task is similar to the idea of diffusion process, which perturb the inputs with pre-defined noise. Concretely, we manually add Gaussian and uniform noise with different intensities to H36M testing set, and evaluate PADS’s performance on this augmented noisy dataset in terms of MPJPE before and after denoising action. Table 3 reveals the experimental results, and we can see that PADS can cope with different types and intensities of noise efficiently. For large intensity noise, PADS tend to take more sampling steps to denoise, which aligns with our design scheme.

Masked Body Parts	MPJPE ↓
Right Leg	17.1
Left Leg	18.8
Right Arm	32.6
Left Arm	30.3
Two Legs	63.3
Two Arms	72.8
Spine	4.5

Table 4: Pose completion results on H36M dataset, which is reported with MPJPE (mm). *Leg* consists of hip, knee, and foot. *Arm* consists of shoulder, elbow, and wrist. *Spine* consists of hip, thorax, and neck.

4.5 Pose Completion

The forward model for pose completion is joint-wise inpainting through a masking matrix, similar to the inpainting task in image restoration domain.

$$\mathbf{y} \sim \mathcal{N}(\mathbf{y} \mid \mathbf{M}\mathbf{x}, \sigma^2\mathbf{I}) \quad (9)$$

where $\mathbf{M} \in \{0, 1\}^{n \times n}$ is the masking matrix. In the experiment setup, we mask out different parts formed by multiple joints. Table 4 shows the reconstruction results. Generally speaking, PADS yields satisfying results when sending in partial observed skeleton. More precisely, we can see that upper body is more difficult to reconstruct than lower body, likely caused by the fact that arms are less constrained by rest of the body and thus have greater degrees of freedom. The superior performance of spine reconstruction can also be attributed to that it is well-constrained by other body joints.

4.6 Ablation Study

Effect of Diffusion Sampler. We first evaluate the performance of our method under different diffusion sampler settings. The comparison is conducted between three different backbones, the Score Matching Network [Song *et al.*, 2020c], DDPM[Ho *et al.*, 2020], and DDIM[Song *et al.*, 2020a], where all models are evaluated on H36M dataset and with

Diffusion Sampler	MPJPE ↓	PA-MPJPE ↓
Score Matching	64.0	47.1
DDPM	65.3	47.4
DDIM (Ours)	41.5	33.1

Table 5: 3D HPE quantitative results on H36M dataset by using different diffusion sampler.

Init. Strategy	Number Iter.	MPJPE ↓	PA-MPJPE ↓
Random Noise	100	242.3	166.8
	250	80.7	60.1
	450	64.1	48.3
	1000	79.4	54.6
Inverse Proj.	100	54.6	39.8
	250	42.6	34.5
	450 (Ours)	41.5	33.1
	1000	63.8	41.0

Table 6: 3D HPE quantitative results on H36M dataset by using different pose initialization strategies and number of sampling iterations.

the same configuration and training scheme. As shown in table 5, despite DDIM having the best performance in terms of both MPJPE and PA-MPJPE, using the other two samplers can also achieve relatively good performance compared with previously shown learning and optimization-based methods. This phenomenon validates the generality of our idea, regardless of the specific structure of the diffusion sampler.

Pose Initialization Strategy Analysis. As introduced in Sec.3.5, we select the initial pose as the inverse projection of input 2D pose given the skeleton root joint’s global trajectory. We argue that this strategy can provide better initialization that aligns with the target 2D pose compared with random noise initialization, thus requiring fewer diffusion steps to output final 3D pose. To certify this design choice, we implement ablation studies on how different initialization strategies along with the number of sampling iterations influence general performance on H36M dataset. We divide the configurations into 2 groups row-wise and use the control variates technique to evaluate the impact and choice of each configuration. Table 6 indicates that the inverse projection outperforms random noise initialization strategy meanwhile needing fewer iterations of sampling.

Impact of Global Trajectory Information. Depth is critical in perspective projection because it determines the scale of 2D measurement in image space. PADS takes ground truth global trajectory as input, whose intuition is that the kinematic constraints we learned are based on the scale of plausible human bodies. If we set the depth at random, the scale of the corresponding 3D pose might deviate from reasonable ones too much, thus making the learned prior useless during sampling. To validate our concern, we conduct ablation studies on manually setting the global trajectory for 3D poses instead of using ground truth. Table 7 shows that the closer the manual set depth is to the ground truth, the better the performance is (on H36M dataset, the average depth is 5.4m),

Pelvis Root Depth	MPJPE ↓	PA-MPJPE ↓
1	420.7	172.8
2	147.5	91.5
5	73.4	52.7
6	84.0	56.6
10	231.3	154.9
GT depth (Ours)	41.5	33.1

Table 7: 3D HPE quantitative results on H36M dataset by inputting different global distance of pelvis root.

Inv. Problem Solver	MPJPE ↓	PA-MPJPE ↓
MCG	80.0	56.1
PIGDM	177.1	75.5
DPS (Ours)	41.5	33.1

Table 8: 3D HPE quantitative results on H36M dataset by using different diffusion-based inverse problem solver.

which reveals that our system is scale-sensitive.

Inverse Problem Solver Analysis. We further replace the DPS inverse problem solver with other state-of-the-art methods like manifold constrained gradients (MCG) [Chung *et al.*, 2022b] and pseudoinverse-guided diffusion models (PIGDM) [Song *et al.*, 2022]). For a fair comparison, all methods use exactly the same pose synthesis model. As shown in Table 8, the choice of solvers have huge impact on the final results and DPS outperforms others in terms of all evaluation metrics. We attribute these results to the domain characteristics of human pose estimation task and the perspective projection operator, whose detail analysis will be a potential research direction in our future work.

5 Conclusions

In this paper, we have proposed PADS, a novel framework which formulates human pose analysis as general inverse problems and solve multiple downstream tasks in a unified pipeline. By leveraging the powerful modeling capability of diffusion models, we effectively learn the kinematic constraints of human skeleton from 3D pose data. During inference, the learned prior will be incorporated as additional constraints and optimize for the corresponding 3D pose through a sequence of conditional denoising processes. This work represents the first diffusion-based framework for tackling various 3D pose-related scenarios in zero-shot manner. Known limitations of this work will the subjects of future research: 1) PADS only validates its feasibility in pose-based representation, this framework has the potential to generalize well across more human representations with better modeling capability, like mesh, implicit functions, etc. 2) DPS solver that we are using is originally designed for image domain inverse problems, and a tailored solver specifically designed for the task of human pose analysis will likely boost the performance.

References

- [Bogo *et al.*, 2016] Federica Bogo, Angjoo Kanazawa, Christoph Lassner, Peter Gehler, Javier Romero, and Michael J Black. Keep it smpl: Automatic estimation of 3d human pose and shape from a single image. In *Computer Vision—ECCV 2016: 14th European Conference, Amsterdam, The Netherlands, October 11–14, 2016, Proceedings, Part V 14*, pages 561–578. Springer, 2016.
- [Chen *et al.*, 2019] Ching-Hang Chen, Ambrish Tyagi, Amit Agrawal, Dylan Drover, Rohith Mv, Stefan Stojanov, and James M Rehg. Unsupervised 3d pose estimation with geometric self-supervision. In *Proceedings of the IEEE/CVF Conference on Computer Vision and Pattern Recognition*, pages 5714–5724, 2019.
- [Chen *et al.*, 2023] Shoufa Chen, Peize Sun, Yibing Song, and Ping Luo. Diffusiondet: Diffusion model for object detection. In *Proceedings of the IEEE/CVF International Conference on Computer Vision*, pages 19830–19843, 2023.
- [Choi *et al.*, 2021] Jooyoung Choi, Sungwon Kim, Yonghyun Jeong, Youngjune Gwon, and Sungroh Yoon. Ilvr: Conditioning method for denoising diffusion probabilistic models. *arXiv preprint arXiv:2108.02938*, 2021.
- [Chung *et al.*, 2022a] Hyungjin Chung, Jeongsol Kim, Michael T Mccann, Marc L Klasky, and Jong Chul Ye. Diffusion posterior sampling for general noisy inverse problems. *arXiv preprint arXiv:2209.14687*, 2022.
- [Chung *et al.*, 2022b] Hyungjin Chung, Byeongsu Sim, Do-hoon Ryu, and Jong Chul Ye. Improving diffusion models for inverse problems using manifold constraints. *Advances in Neural Information Processing Systems*, 35:25683–25696, 2022.
- [Ci *et al.*, 2023] Hai Ci, Mingdong Wu, Wentao Zhu, Xiaoxuan Ma, Hao Dong, Fangwei Zhong, and Yizhou Wang. Gfpose: Learning 3d human pose prior with gradient fields. In *Proceedings of the IEEE/CVF Conference on Computer Vision and Pattern Recognition*, pages 4800–4810, 2023.
- [Davydov *et al.*, 2022] Andrey Davydov, Anastasia Remizova, Victor Constantin, Sina Honari, Mathieu Salzmann, and Pascal Fua. Adversarial parametric pose prior. In *Proceedings of the IEEE/CVF Conference on Computer Vision and Pattern Recognition*, pages 10997–11005, 2022.
- [Hatze, 1997] H Hatze. A three-dimensional multivariate model of passive human joint torques and articular boundaries. *Clinical Biomechanics*, 12(2):128–135, 1997.
- [Ho and Salimans, 2022] Jonathan Ho and Tim Salimans. Classifier-free diffusion guidance. *arXiv preprint arXiv:2207.12598*, 2022.
- [Ho *et al.*, 2020] Jonathan Ho, Ajay Jain, and Pieter Abbeel. Denoising diffusion probabilistic models. *Advances in neural information processing systems*, 33:6840–6851, 2020.
- [Ionescu *et al.*, 2013] Catalin Ionescu, Dragos Papava, Vlad Olaru, and Cristian Sminchisescu. Human3.6m: Large scale datasets and predictive methods for 3d human sensing in natural environments. *IEEE transactions on pattern analysis and machine intelligence*, 36(7):1325–1339, 2013.
- [Ji *et al.*, 2023] Haorui Ji, Hui Deng, Yuchao Dai, and Hongdong Li. Unsupervised 3d pose estimation with non-rigid structure-from-motion modeling. *arXiv preprint arXiv:2308.10705*, 2023.
- [Jiang *et al.*, 2022] Zhongyu Jiang, Haorui Ji, Samuel Menaker, and Jenq-Neng Hwang. Golfpose: Golf swing analyses with a monocular camera based human pose estimation. In *2022 IEEE International Conference on Multimedia and Expo Workshops (ICMEW)*, pages 1–6. IEEE, 2022.
- [Jiang *et al.*, 2023] Zhongyu Jiang, Zhuoran Zhou, Lei Li, Wenhao Chai, Cheng-Yen Yang, and Jenq-Neng Hwang. Back to optimization: Diffusion-based zero-shot 3d human pose estimation. *arXiv preprint arXiv:2307.03833*, 2023.
- [Kanazawa *et al.*, 2018] Angjoo Kanazawa, Michael J Black, David W Jacobs, and Jitendra Malik. End-to-end recovery of human shape and pose. In *Proceedings of the IEEE conference on computer vision and pattern recognition*, pages 7122–7131, 2018.
- [Kawar *et al.*, 2022] Bahjat Kawar, Michael Elad, Stefano Ermon, and Jiaming Song. Denoising diffusion restoration models. *Advances in Neural Information Processing Systems*, 35:23593–23606, 2022.
- [Kocabas *et al.*, 2020] Muhammed Kocabas, Nikos Athanasiou, and Michael J Black. Vibe: Video inference for human body pose and shape estimation. In *Proceedings of the IEEE/CVF conference on computer vision and pattern recognition*, pages 5253–5263, 2020.
- [Li *et al.*, 2022] Wenhao Li, Hong Liu, Hao Tang, Pichao Wang, and Luc Van Gool. Mhformer: Multi-hypothesis transformer for 3d human pose estimation. In *Proceedings of the IEEE/CVF Conference on Computer Vision and Pattern Recognition*, pages 13147–13156, 2022.
- [Li *et al.*, 2023] Xin Li, Yulin Ren, Xin Jin, Cuiling Lan, Xingrui Wang, Wenjun Zeng, Xinchao Wang, and Zhibo Chen. Diffusion models for image restoration and enhancement—a comprehensive survey. *arXiv preprint arXiv:2308.09388*, 2023.
- [Loper *et al.*, 2023] Matthew Loper, Naureen Mahmood, Javier Romero, Gerard Pons-Moll, and Michael J Black. Smpl: A skinned multi-person linear model. In *Seminal Graphics Papers: Pushing the Boundaries, Volume 2*, pages 851–866. 2023.
- [Ma *et al.*, 2023] Yue Ma, Yingqing He, Xiaodong Cun, Xintao Wang, Ying Shan, Xiu Li, and Qifeng Chen. Follow your pose: Pose-guided text-to-video generation using pose-free videos. *arXiv preprint arXiv:2304.01186*, 2023.

- [Martinez *et al.*, 2017] Julieta Martinez, Rayat Hossain, Javier Romero, and James J Little. A simple yet effective baseline for 3d human pose estimation. In *Proceedings of the IEEE international conference on computer vision*, pages 2640–2649, 2017.
- [Mehta *et al.*, 2017] Dushyant Mehta, Helge Rhodin, Dan Casas, Pascal Fua, Oleksandr Sotnychenko, Weipeng Xu, and Christian Theobalt. Monocular 3d human pose estimation in the wild using improved cnn supervision. In *2017 international conference on 3D vision (3DV)*, pages 506–516. IEEE, 2017.
- [Novotny *et al.*, 2019] David Novotny, Nikhila Ravi, Benjamin Graham, Natalia Neverova, and Andrea Vedaldi. C3dpo: Canonical 3d pose networks for non-rigid structure from motion. In *Proceedings of the IEEE/CVF International Conference on Computer Vision*, pages 7688–7697, 2019.
- [Pavlo *et al.*, 2019] Dario Pavlo, Christoph Feichtenhofer, David Grangier, and Michael Auli. 3d human pose estimation in video with temporal convolutions and semi-supervised training. In *Proceedings of the IEEE/CVF conference on computer vision and pattern recognition*, pages 7753–7762, 2019.
- [Poole *et al.*, 2022] Ben Poole, Ajay Jain, Jonathan T Barron, and Ben Mildenhall. Dreamfusion: Text-to-3d using 2d diffusion. *arXiv preprint arXiv:2209.14988*, 2022.
- [Rombach *et al.*, 2022] Robin Rombach, Andreas Blattmann, Dominik Lorenz, Patrick Esser, and Björn Ommer. High-resolution image synthesis with latent diffusion models. In *Proceedings of the IEEE/CVF conference on computer vision and pattern recognition*, pages 10684–10695, 2022.
- [Shan *et al.*, 2023] Wenkang Shan, Zhenhua Liu, Xinfeng Zhang, Zhao Wang, Kai Han, Shanshe Wang, Siwei Ma, and Wen Gao. Diffusion-based 3d human pose estimation with multi-hypothesis aggregation. *arXiv preprint arXiv:2303.11579*, 2023.
- [Song *et al.*, 2020a] Jiaming Song, Chenlin Meng, and Stefano Ermon. Denoising diffusion implicit models. *arXiv preprint arXiv:2010.02502*, 2020.
- [Song *et al.*, 2020b] Jie Song, Xu Chen, and Otmar Hilliges. Human body model fitting by learned gradient descent. In *European Conference on Computer Vision*, pages 744–760. Springer, 2020.
- [Song *et al.*, 2020c] Yang Song, Jascha Sohl-Dickstein, Diederik P Kingma, Abhishek Kumar, Stefano Ermon, and Ben Poole. Score-based generative modeling through stochastic differential equations. *arXiv preprint arXiv:2011.13456*, 2020.
- [Song *et al.*, 2022] Jiaming Song, Arash Vahdat, Morteza Mardani, and Jan Kautz. Pseudoinverse-guided diffusion models for inverse problems. In *International Conference on Learning Representations*, 2022.
- [Stenum *et al.*, 2021] Jan Stenum, Kendra M Cherry-Allen, Connor O Pyles, Rachel D Reetzke, Michael F Vignos, and Ryan T Roemmich. Applications of pose estimation in human health and performance across the lifespan. *Sensors*, 21(21):7315, 2021.
- [Tevet *et al.*, 2022] Guy Tevet, Sigal Raab, Brian Gordon, Yonatan Shafir, Daniel Cohen-Or, and Amit H Bermano. Human motion diffusion model. *arXiv preprint arXiv:2209.14916*, 2022.
- [Wandt *et al.*, 2022] Bastian Wandt, James J Little, and Helge Rhodin. Elepose: Unsupervised 3d human pose estimation by predicting camera elevation and learning normalizing flows on 2d poses. In *Proceedings of the IEEE/CVF Conference on Computer Vision and Pattern Recognition*, pages 6635–6645, 2022.
- [Wang and Lucey, 2021] Chaoyang Wang and Simon Lucey. Paul: Procrustean autoencoder for unsupervised lifting. In *Proceedings of the IEEE/CVF Conference on Computer Vision and Pattern Recognition*, pages 434–443, 2021.
- [Weng *et al.*, 2019] Chung-Yi Weng, Brian Curless, and Ira Kemelmacher-Shlizerman. Photo wake-up: 3d character animation from a single photo. In *Proceedings of the IEEE/CVF conference on computer vision and pattern recognition*, pages 5908–5917, 2019.
- [Yu *et al.*, 2021] Zhenbo Yu, Bingbing Ni, Jingwei Xu, Junjie Wang, Chenglong Zhao, and Wenjun Zhang. Towards alleviating the modeling ambiguity of unsupervised monocular 3d human pose estimation. In *Proceedings of the IEEE/CVF International Conference on Computer Vision*, pages 8651–8660, 2021.
- [Yuan *et al.*, 2023] Ye Yuan, Jiaming Song, Umar Iqbal, Arash Vahdat, and Jan Kautz. Physdiff: Physics-guided human motion diffusion model. In *Proceedings of the IEEE/CVF International Conference on Computer Vision*, pages 16010–16021, 2023.
- [Zeng *et al.*, 2022] Haitian Zeng, Xin Yu, Jiayu Miao, and Yi Yang. Mhr-net: Multiple-hypothesis reconstruction of non-rigid shapes from 2d views. In *Computer Vision—ECCV 2022: 17th European Conference, Tel Aviv, Israel, October 23–27, 2022, Proceedings, Part II*, pages 1–17. Springer, 2022.
- [Zhang *et al.*, 2022] Jinlu Zhang, Zhigang Tu, Jianyu Yang, Yujin Chen, and Junsong Yuan. Mixste: Seq2seq mixed spatio-temporal encoder for 3d human pose estimation in video. In *Proceedings of the IEEE/CVF conference on computer vision and pattern recognition*, pages 13232–13242, 2022.
- [Zhang *et al.*, 2023] Lvmin Zhang, Anyi Rao, and Maneesh Agrawala. Adding conditional control to text-to-image diffusion models. In *Proceedings of the IEEE/CVF International Conference on Computer Vision*, pages 3836–3847, 2023.
- [Zheng *et al.*, 2022] Huangjie Zheng, Pengcheng He, Weizhu Chen, and Mingyuan Zhou. Truncated diffusion probabilistic models and diffusion-based adversarial auto-encoders. *arXiv preprint arXiv:2202.09671*, 2022.